Heliyon 9 (2023) e21574

Contents lists available at ScienceDirect

Heliyon

journal homepage: www.cell.com/heliyon

Research article

Reversal in the drought stress response of the Scots pine forest ecosystem: Local soil water regime as a key to improving climate change resilience

Mikhail I. Bogachev [a,*], Artur M. Gafurov [b], Pavel Y. Iskandirov [b], Dmitrii I. Kaplun [a], Airat R. Kayumov [b], Asya I. Lyanova [a], Nikita S. Pyko [a], Svetlana A. Pyko [a], Anastasiia N. Safonova [a], Aleksandr M. Sinitca [a], Bulat M. Usmanov [b], Denis V. Tishin [a,b,*]

[a] St. Petersburg Electrotechnical University "LETI", 5-F Professor Popov street, St. Petersburg, 197022, Russia
[b] Kazan Federal University, 18 Kremlevskaya street, Kazan, Tatarstan, 420008, Russia

ARTICLE INFO

Keywords:
Climate resilience
Tree-ring width
Drought stress
Hydrological conditions
Detrended partial cross-correlation analysis

ABSTRACT

In a changing climate, forest ecosystems have become increasingly vulnerable to continuously exacerbating heat and associated drought conditions. Climate stress resilience is governed by a complex interplay of global, regional, and local factors, with hydrological conditions being among the key players. We studied a Scots pine (*Pinus sylvestris* L.) forest ecosystem located near the southern edge of the boreal ecotone, which is particularly subjected to frequent and prolonged droughts. By comparing the dendrochronological series of pines growing in apparently contrasting hydrological conditions ranging from the waterlogged peat bog area to the dry soil at the surrounding elevations, we investigated how the soil water regime affects the climate response and drought stress resilience of the forest ecosystem. We found that in the dry land area, a significant fraction of the trees were replaced after two major climate extremes: prolonged drought and extremely low winter temperatures. The latter has also been followed by a three- to ten-fold growth reduction of the trees that survived in the next year, whereas no similar effect has been observed in the peat bog area. Multi-scale detrended partial cross-correlation analysis (DPCCA) indicated that tree-ring width (TRW) was negatively correlated with spring and summer temperatures and positively correlated with the Palmer drought severity index (PDSI) for the same year. For the elevated dry land area, the above effect extends to interannual scales, indicating that prolonged heatwaves and associated droughts are among the factors that limit tree growth. In marked contrast, in the waterlogged peat bog area, a reversed tendency was observed, with prolonged dry periods as well as warmer springs and summers over several consecutive years, leading to increasing tree growth with a one- to three-year time lag. Altogether, our results indicate that the pessimal conditions of a warming climate could become favorable through the preservation of the soil water regime.

* Corresponding author.
E-mail addresses: rogex@yandex.com (M.I. Bogachev), kpfuecology@gmail.com (D.V. Tishin).

https://doi.org/10.1016/j.heliyon.2023.e21574
Received 29 April 2023; Received in revised form 13 October 2023; Accepted 24 October 2023

Available online 29 October 2023

1. Introduction

In a changing climate, the duration of summer heat waves in Europe has doubled, and the number of days during which extreme temperatures have been recorded has tripled since 1880 [1]. The extreme summer temperatures of 2010, accompanied by a major drought in a large part of Eurasia [2] represent a prominent example of recently intensified heatwaves and associated flash droughts [3]. Such anomalies are characterized by an increased demand for evaporation [4], which exacerbates the negative impact of extreme temperatures on ecosystem productivity, vigor, and survival [5].

Forest ecosystems play an indispensable role in the preservation of microclimate conditions essential to the balance of the environment and well-being of the local biome as a whole. Climate exerts the strongest control over the geographic location of ecotones, with coniferous forests located near the southern edge of the boreal ecotone being among the most endangered due to increased environmental pressure [6]. While recent shifts of ecotone boundaries to higher latitudes under climate change could hardly be counteracted, with certain alterations seemingly irreversible at the continental scale, fine-scale drivers play an increasingly important role in the definition of biome boundaries and, thus, in the preservation and well-being of local ecotones [7].

Among prominent examples, Scots pine (*Pinus sylvestris L.*) is very sensitive to summer droughts, and thus pine forests growing near the southern border of the boreal zone could also be considered characteristic bioindicators highly sensitive to hydroclimatic changes and overall environmental pressure [8–10]. Recent and ongoing climate alterations are associated with changes in forest structure and composition that are especially pronounced in the northern latitudes, strongly affecting the southern edge of the boreal ecotone [6]. In recent decades, exacerbating heat and associated drought stress conditions have resulted in significant alterations in boreal forest ecosystems both in Eurasia and North America, including changes in demographic rates, disturbance regimes, and range shifts of some tree species [11,12]. There are certain indications that in some areas, the southern edge of the boreal ecotone already exhibits a northward shift [13], and there are concerns that these alterations could act as a feedforward driver reinforcing the effects of global climate warming, at least on the local and regional scales [14].

With a warming climate and associated drought stress, a decrease in photosynthetic activity significantly limits carbon uptake by the ecosystem. As soils dry out and tree canopy transpiration exceeds water uptake by roots, tree stem water gradually depletes. Depletion of stem water stunts tree growth, further reducing their capacity to absorb carbon. In the short term, the release of water from the trunk's internal reserves can temporarily mitigate the negative impact of drought on the integrity of the tree's vascular system. However, extended periods of drought eventually lead to hydraulic failure, dehydration, and tissue damage, which can lead to tree death due to drought [15–19].

Heat and associated drought stress resilience of endangered forest ecosystems are governed by a complex interplay of global, regional, and local factors. Unraveling these factors and their interactions is of immense importance for a better understanding of ecosystem adaptability, which in turn can be used to improve local environmental management in a changing climate. However, it is often difficult to extract these underlying relationships solely from retrospective data. The impact of particular climate extremes, such as heatwaves, droughts, and extreme freezing temperatures, as well as their consequences, such as forest fires, are often explicitly reflected in tree age distributions. The replacement of significant fractions of trees following extreme events typically leads to characteristic peaks in age distributions [20]. In contrast, evaluating the long-term impacts of prolonged and, especially, multiple climate anomalies, as well as distinguishing their contributions from local factors, often appears more challenging [21].

Long-term persistence in climate variability [22] leads to both the clustering of flash heatwaves and the emergence of prolonged droughts [23], considerably increasing the impact of hydroclimatic anomalies on forest ecosystems. Conventional time-series analysis methods often neglect long-term memory, resulting, for example, in the underestimation of clustering effects in tree-ring-based climate reconstructions [24] and the overestimation of the significance of local trends [25,26].

In recent years, significant progress has been made to overcome these limitations. Dedicated statistical methods, such as detrended fluctuation analysis (DFA) [27] and wavelet transform analysis (WTA) [28], which are capable of adequately quantifying long-term persistence in the presence of additive short-term and/or periodic trends [29] have been applied. The resulting assessments of climate variability records, their tree-ring data-based reconstructions, and surrogate data generated by climate models provided the basis for more adequate mathematical models of their long-term dynamics. Based on these models, the statistical significance of local trends has been re-evaluated [30–32] and corresponding corrections to tree-ring-based climate reconstruction procedures have been proposed [33–35].

In this study, we corroborate the hypothesis that the climate stress resilience of forest ecosystems located near the southern edge of the boreal ecotone, which are particularly vulnerable to increasingly frequent and prolonged droughts, could be improved by preserving the local soil water regime. Therefore, we extended the detrended fluctuation analysis methodology to quantify the interconnections between long-term hydroclimatic variations and tree-ring width data. Using detrended cross-correlation analysis (DCCA) [36], we analyzed how the annual radial growth of trees is associated with the monthly temperature and PDSI variations over the preceding 60 months, from September to August (because tree growth in the considered climate zone typically occurs only between May and August). Using detrended partial cross-correlation analysis (DPCCA) [37], we analyzed partial correlations to distinguish between the contributions of climate change and effects of aging on tree growth. For this purpose, we adapt the existing D(P)CCA methodology to detrend in gliding rather than non-overlapping windows, and combine this method with an alternative central moving average (CMA)-based detrended fluctuation analysis procedure [38], both aiming at the minimization of discontinuity in the residuals.

Table 1
Spectral channels used in the remote sensing analysis.

Channel	Center ± bandwidth, nm
BLUE	475 ± 32
GREEN	560 ± 27
RED	668 ± 16
Red edge (RE)	717 ± 12
Near-infrared (NIR)	842 ± 57

2. Materials and methods

2.1. Study area

The study area is located in the Volzhsko-Kamsky State Nature Biosphere Reserve on the left bank of the Volga River, 30 km west of Kazan City, Republic of Tatarstan, Russia, near the southern edge of the boreal ecotone [40]. The landscape exhibits a dune-hilly character with hollows and ancient beams, with absolute elevations between 65 m and 105 m. The soil was sandy and medium podzolic. Peat bogs of limnogenic origin are typically located in the interdune depressions. The main species are Scots pines (*Pinus sylvestris* L.), which account for up to 70% of the forested area and are found in various habitats, from waterlogged peat bogs to dry land.

Our study focused on the local area of the "Dolgoe" sphagnum bog (N 55.900190, E 48.821186), which is characterized by peat thickness of up to 3.5 m, and a surrounding elevated dry land area (considered a relevant control). The pine forest in the peat bog area is dominated by *Pinus sylvestris* L. with single trees of *Betula pendula* Roth. Ground vegetation is represented by *Oxycoccus palustris*, *Chamaedaphne calyculata*, *Rhododendron tomentosum*, and *Andromeda polifolia* L., with a predominance of sphagnum mosses (*Sphagnum* sp.) [41]. The study area shown in Fig. 1 is characterized by an elevation gradient that leads to a respective gradient in local hydrological conditions. While the most pronounced contrast can be observed between the elevated dry land surrounding the peat bog and the peat bog area itself, there is also a less pronounced decline in elevation between the western and eastern parts of the peat bog area itself. Because Scots pine trees in the studied peat bog area tend to cluster, forming local micropopulations, we analyzed sample trees from three separate locations within the peat bog area ($n = 32$ in the western, $n = 26$ in the central, and $n = 42$ in the eastern parts, with presumable differences in the local hydrological regimes due to the elevation gradient). In addition, three locations on the elevated dry land surrounding the peat bog area were chosen as controls. Because there were no major contrasts between local conditions at these locations, we considered them as a single control group (together in three sites). The locations of the selected trees, as well as local elevations at each site, are shown in Fig. 1).

2.2. Tree-ring measurements

Tree sampling was performed according to the methodology adopted in an earlier dendrochronological study [42]. Cores were extracted from the sample trees using a Pressler borer. Because of the relatively small diameters of the trees, especially in the peat bog area, and only moderate local terrain slopes, only one core per tree was collected, predominantly from the south-facing direction.

The tree ring width (TRW) was measured on a Lintab-6 using the TSAPWin software package [43]. The quality of the cross-chronologies was assessed using Cofecha software [44]. The exact location of each tree was determined using a Garmin GPSMAR 62S GPS receiver, as shown in Fig. 1.

2.3. Meteorological data sources

Average monthly temperature variations were obtained from the RIHMI-WDC Baseline Climatological Database http://meteo.ru/english/data (the data series for the nearest station can be found under World Meteorological Organization (WMO) ID 27595) [45]. The CRU self-calibrated Palmer Drought Severity Index (PDSI) data have been obtained from the KNMI Climate Explorer available online at https://climexp.knmi.nl/ (Monthly observations → CRU self-calibrated PDSI) [46,47], assessed using the coordinate points in the center of the studied area (see above) also with monthly resolution (available since 1901).

2.4. Multispectral remote sensing

Remote sensing imagery was acquired using a Geoscan 401 Geodesy UAV equipped with a MicaSense RedEdge-MX (RX02 series) multi-spectral camera (pixel size 3.75 μm, resolution 1280 × 960 (1.2 MP ×5 imagers), aspect ratio 4:3, sensor size 4.8 mm ×3.6 mm, focal length 5.4 mm, field of view: 47.2°, 35.4° vertical, output depth 12 bit). The recorded channels are listed in Table 1.

Based on the multispectral remote observation data, the following vegetation indices were calculated (for a more detailed description, please refer to [48–52], see also [53–55] and references therein):

- **Enhanced vegetation index (EVI)**

$$EVI = \frac{2.5 \cdot (NIR - RED)}{NIR + 6 \cdot RED - 7.5 \cdot BLUE + 1} \quad (1)$$

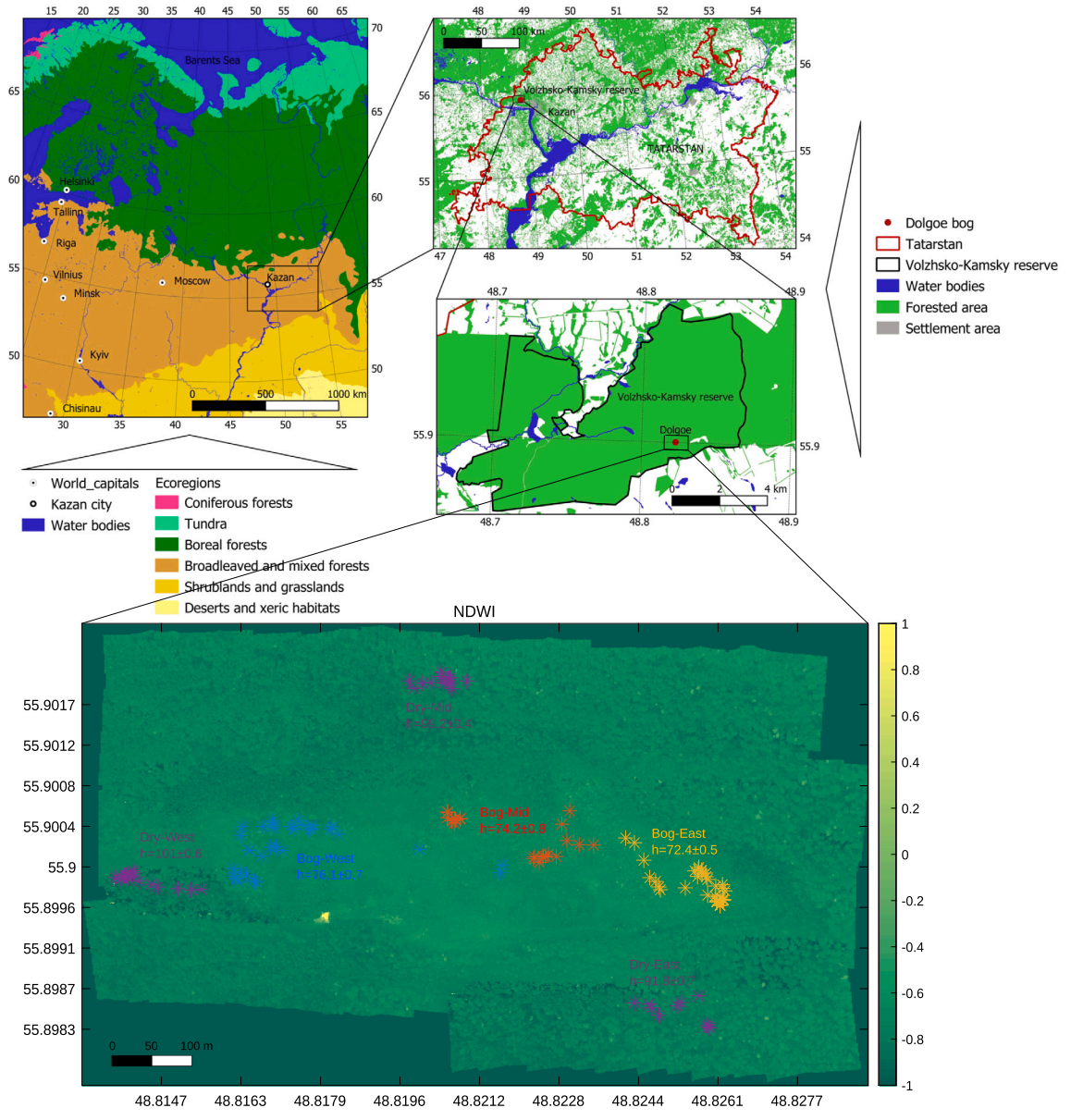

Fig. 1. Overview of the study area with marked-up tree locations. The geographical location in the upper panel was prepared using QGIS software based on OpenStreetMap data. Ecoregions were classified according to a previous study [39]. The background in the lower panel represents the NDWI (for details, see Sec. 2.4) obtained using multispectral imaging.

a modification of the conventional Normalized Difference Vegetation Index (NDVI) that effectively displays greenness (associated with the relative biomass). While the conventional NDVI index takes advantage of the contrast between the characteristics of the chlorophyll pigment absorption in the red band and the high reflectivity of plant materials in the NIR band, the EVI additionally accounts for atmospheric influences and vegetation background signals, making it less sensitive to background and atmospheric noise and reducing saturation for areas with dense green vegetation.

- **Normalized difference water index**

$$NDWI = \frac{GREEN - NIR}{GREEN + NIR} \tag{2}$$

an index originally suggested in [56] to quantify water content is simply reciprocal to the Green Normalized Difference Vegetation Index (GNDVI), another widely adopted vegetation index that determines water and nitrogen uptake into the plant canopy.

- **Red-edge triangulated vegetation index (RTVICore)**

$$RTVICore = 100 \cdot (NIR - RE) - 10 \cdot (NIR - GREEN) \tag{3}$$

a three-band vegetation index was used to estimate the leaf area index and biomass. This index uses reflectance in the NIR, red-edge, and green spectral bands.

- **Modified triangular vegetation index (MTVI2)**

$$MTVI2 = 1.5 \cdot (1.2 \cdot (NIR - GREEN)) - 2.5 \cdot (RED - GREEN) \times \sqrt{(2 \cdot NIR + 1)^2 - (6 \cdot NIR - 5\sqrt{RED}) - 0.5} \tag{4}$$

a vegetation index for detecting leaf chlorophyll content at the canopy scale while being relatively insensitive to the leaf area index. It uses the reflectance in the green, red, and NIR bands.

In this study, we used the NDWI index, calculated as shown in Eq. (2) [56] to quantify the local variations in the relative water content in the soil over the study area, because conventional methods to measure water content in the soil moisture could not be applied in the peat bog area due to saturation. In addition, the EVI, RTVICore, and MTVI2 indices reflected the status of vegetation at the time of observation (August 17, 2022).

2.5. Time series analysis

We employed detrending fluctuation analysis methods, which have been recommended as appropriate tools for analyzing long-term tree-ring data and respective climate reconstructions. Recently, the capability of these methods to overcome the inevitable drawbacks of conventional correlation analysis when applied to long-term correlated data series, including nonstationary regimes, has been demonstrated in several studies [33,34,57]. In this study, we follow this direction and apply the recently proposed D(P)CCA method [36,37] to analyze cross-correlations between tree-ring data and climate variations.

2.5.1. Detrended fluctuation analysis

To quantify the long-term persistence of the annual tree-ring data and hydroclimatic variations, we employed modifications of the widely adopted detrended fluctuation analysis (DFA) methods [27]. To distinguish between short- and long-term effects and detect a possible delayed response of the forest ecosystem to climate variations, we used multi-scale fluctuation analysis to extract relevant information from the observational data.

Technically, multi-scale fluctuation analysis does not deal directly with the observational data series x_i, but with their cumulative sums $X_i \equiv \sum_{k=1}^{i} x_k$, where $i = 1, \dots, L$ is the data sample, and L is the length of the data, also known as "profiles" [58,38]. In the context of the TRW series, the profile represents the cumulative tree growth over its entire lifespan. To focus on the relative effects characterized by TRW fluctuations without loss of generality, we can subtract the average from the raw data series and calculate the profile for x_i^0 instead of x_i, such that upward and downward trends indicate increasing and decreasing growth rates, respectively [57].

Next, the profiles are split into K_s time windows of length s. In conventional fluctuation analysis (FA), one considers the mean square displacements over all windows of size s

$$F_\nu^2(s) = [X(\nu s) - X((\nu - 1)s)]^2 \tag{5}$$

where ν is the window number, and is averaged over all K_s segments for each window size s to obtain the fluctuation function $F(s)$

$$F^2(s) \equiv \frac{1}{K_s} \sum_{\nu=1}^{K_s} F_\nu^2(s) \tag{6}$$

In the DFA procedure, in each window, the least mean squares polynomial $p_{\nu,i}$ that fits to the profile is calculated, representing local trends in growth over s years. By subtracting the polynomial fits $p_{\nu,i}$ one obtains the fluctuations around the profile and calculates statistics to (5) and (6) as

$$F_\nu^2(s) \equiv \frac{1}{s} \sum_{i=1}^{s} \left[X_{(\nu-1)s+i} - p_{\nu,i}\right]^2 \tag{7}$$

followed by averaging $F_\nu^2(s)$ over all K_s windows

$$F^2(s) \equiv \frac{1}{K_s} \sum_{\nu=1}^{K_s} F_\nu^2(s) \tag{8}$$

For long-term correlated data, the DFA fluctuation function increases by a power law as $F(s) \propto s^H$, where H is the Hurst exponent, irrespective of the order of the detrending polynomial. In the simple case of fully random ("white noise") increments $H = 1/2$, while $H > 1/2$ correspond to positively and $H < 1/2$ to negatively correlated increments, respectively [58].

Although DFA is known for its robustness over long timescales, providing reliable estimates up to $s \lesssim L/4$, it is not applicable on short time scales because of the exact or near-exact fitting problem. Even for noise-free simulated data, asymptotic behavior can be

observed only at $s \gtrsim 8$. The latter is why DFA is often combined with wavelet transform analysis (WTA) to cover all scales (for more details, see, e.g., [59,57] and references therein). In the WTA procedure, the observational data series x_i were split into windows of size s, and local sums $X_{\nu,s} \equiv \sum_{k=1}^{s} x_k$ were calculated for each window ν, resembling the standard FA procedure. In high-order WTAp, further detrending is based on an analysis of the statistics of the p-th differences in the local sums $X_{\nu,s}$. The latter results in WTA being considerably less noise-robust than DFA, especially at large scales, providing relevant estimates only at $1 \le s \lesssim L/100$, according to the results of simulation-based studies (see, e.g., [59] and references therein).

In their conventional implementations, both DFA and WTA procedures consider non-overlapping time windows resulting in discontinuity in the series of residuals, a common drawback that has been reduced in the central moving average (CMA)-based detrended fluctuation analysis [38], where local polynomial fits $p_{\nu,i}$ have been replaced by the local averages $\overline{X_\nu}$, and non-overlapping windows of length s by moving windows of the same size, such that the residuals are calculated as $Y_{\nu,k} = X_{\nu,k} - \overline{X_{\nu,k}}$. In terms of the effective scale range and noise robustness, CMA occupies an intermediate position between the DFA and WTA methods and thus could be considered an all-scale substitute for the combination of the above two methods. For the surrogate data, CMA provides reasonable approximations to asymptotic behavior already at small scales, at least for odd window sizes, such that there is no bias of the central point in the window due to discreteness.

Because individual dendrochronological series are characterized by different lengths and locations on the time scale representing the life cycles of each tree, they only partially overlap. Thus, to avoid further loss of data from splitting into non-overlapping windows, we applied both DFA and CMA in gliding windows of sizes s with single-year steps.

2.5.2. Detrended cross-correlation analysis

To quantify the relative dynamics, the above DFA (or CMA) procedures can be generalized to the analysis of several simultaneously observed time series x_i^j. For this, pairwise covariances between the residual series (after subtraction of the average or polynomial fit, respectively) are calculated as [36,37]

$$F^2_{j_1,j_2}(s) \equiv \frac{\sum_{l=1}^{(N-s)(s+1)} Y_l^{j_1} Y_l^{j_2}}{(N-s)(s+1)} \tag{9}$$

Next, for all $j_1, j_2 = 1, \dots, m$ one obtains the covariance matrix, yielding

$$F^2(s) = \begin{bmatrix} F^2_{1,1}(s) & F^2_{1,2}(s) & \dots & F^2_{1,m}(s) \\ F^2_{2,1}(s) & F^2_{2,2}(s) & \dots & F^2_{2,m}(s) \\ \dots & \dots & \dots & \dots \\ F^2_{m,1}(s) & F^2_{m,2}(s) & \dots & F^2_{m,m}(s) \end{bmatrix} \tag{10}$$

While the diagonal elements of the matrix $F^2_{j,j}(s)$ are simple variances and correspond to the fluctuation functions $F^2(s)$ in the conventional DFA (or CMA) [27,38], non-diagonal elements of the fluctuation matrix $F^2_{j_1,j_2}(s)$ represent cross-covariances. To obtain cross-correlations between data series j_1 and j_2 (for example, between the annual tree-ring data and hydroclimatic variations), we calculate [36,37]

$$R_{j_1,j_2}(s) \equiv \frac{F^2_{j_1,j_2}(s)}{\sqrt{F^2_{j_1,j_1}(s) \cdot F^2_{j_2,j_2}(s)}} \tag{11}$$

and obtains the matrix of cross-correlation coefficients by normalization, yielding

$$R(s) = \begin{bmatrix} R_{1,1}(s) & R_{1,2}(s) & \dots & R_{1,m}(s) \\ R_{2,1}(s) & R_{2,2}(s) & \dots & R_{2,m}(s) \\ \dots & \dots & \dots & \dots \\ R_{m,1}(s) & R_{m,2}(s) & \dots & R_{m,m}(s) \end{bmatrix} \tag{12}$$

Finally, to exclude spurious correlations induced by cross-modulation of the analyzed time series, partial correlation coefficients can also be obtained by calculating the inverse of the cross-correlation coefficient matrix, yielding

$$C(s) = R^{-1}(s) = \begin{bmatrix} C_{1,1}(s) & C_{1,2}(s) & \dots & C_{1,m}(s) \\ C_{2,1}(s) & C_{2,2}(s) & \dots & C_{2,m}(s) \\ \dots & \dots & \dots & \dots \\ C_{m,1}(s) & C_{m,2}(s) & \dots & C_{m,m}(s) \end{bmatrix} \tag{13}$$

followed by normalization as

$$P_{j_1,j_2}(s) = \frac{-C_{j_1,j_2}(s)}{\sqrt{C_{j_1,j_1}(s) \cdot C_{j_2,j_2}(s)}} \tag{14}$$

where the latter coefficients characterize the intrinsic correlations between data series j_1 and j_2.

While in the original work [37], the above procedure was formulated for the DFA-based detrending, in this work, we also apply a similar procedure to the fluctuations obtained by CMA-based detrending. Finally, to account for a possible delayed response of the

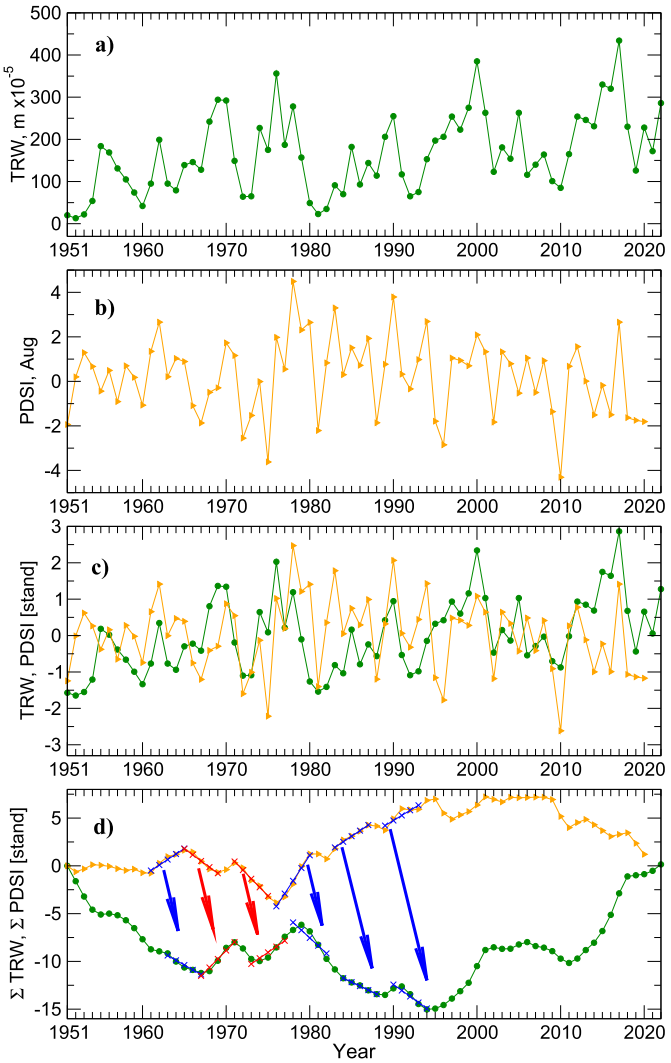

Fig. 2. A simple illustration of the CMA-based multi-scale detrended cross-correlation analysis procedure: (a) TRW and (b) PDSI data series are first standardized by subtracting their averages and dividing by standard deviations (c). Next, cumulative profiles (d) are calculated, and local windows of size s are determined. In each window, the local mean is calculated and subtracted, resulting in an estimate of the relative trend around the local mean. Panel (d) exemplifies the correspondence between the variations in the PDSI index with local increasing (blue) and negative (red) trends indicating shifts toward more humid and dry conditions, respectively, and local trends in a single representative TRW profile corresponding to either an increasing (red) or decreasing (blue) annual growth rate with a two-year delay.

tree growth rates to hydroclimatic variations, we analyzed not only synchronous but also delayed cross-correlations [60] with time lags of up to five years. To distinguish between the effects of tree aging and climate change, we obtained partial correlations using modified DPCCA (but with CMA-based detrending) for the annual observations of TRW, tree age, and climate variations (temperature or PDSI, respectively). In this way, linear associations with tree age are eliminated from cross-correlations between TRW and climate variations, separately for each of the studied trees.

Fig. 2 illustrates the CMA-based multi-scale detrended cross-correlation analysis procedure. In this example, the dominance of negative correlations between the PDSI variations taken for August each year and a single TRW data series for tree Nr. 115, at scale $s = 5$, with a 2-year delay lag, is demonstrated. The covariances F_{ij} and cross-correlation coefficients R_{ij} are next calculated by averaging over *all* positions of the local time window of the same duration $s = 5$ years and a 2-year time lag between the analyzed records.

2.6. Statistical significance testing

To reveal statistically significant discrepancies between measurements obtained for different local subareas, we employed the one-way non-parametric Kruskal-Wallis statistical test with a significance threshold of $p = 0.05$. In multi-group comparison scenarios, to specify particular contributors to the overall discrepancies, we also performed post hoc analysis using the Mann-Whitney U-test with the same confidence threshold level.

3. Results

3.1. Multispectral remote sensing

We used multispectral imaging to characterize the local hydrological conditions, which in turn affect the overall vegetation. Figures S1 and S2 in the Supplementary Material show that the vegetation indices (EVI, RTVICore, and MTVI2) generally follow the elevation profile, with the highest values observed for the elevated dry land area surrounding the peat bog and reduced values for the peat bog, with a tendency of monotonous reduction with lowering elevation both within and outside of the peat bog. The NDWI index (also represented in Fig. 1), as expected, shows a reciprocal pattern, with a clear trend indicating increase in water content with decreasing elevation. Figure S2 shows boxplots indicating discrepancies between the local measurements in each of the four studied areas (western, middle, and eastern parts of the peat bog, with continuously decreasing elevation, as well as dry land sites at the surrounding elevations as a single control group), including five multispectral bands (Blue, Green, Red, RedEdge, NIR), as well as calculated vegetation indices (EVI, NDWI, RTVICore, MTVI2). In Fig. S2, statistically significant discrepancies are indicated by (red) annotation, with reported p-values according to a one-way non-parametric Kruskal-Wallis statistical test, while particular locations where respective measurements indicated significant discrepancies with the dry land (according to the post hoc test results) are denoted by (red) asterisks.

3.2. Tree-ring data and hydroclimatic time series

Fig. 3 shows dendrochronological data series (the first three series obtained by averaging over each of the three locations within the peat bog area and the fourth series obtained by averaging over all three locations in the surrounding dry land area, with the latter acting as relevant control, are provided), as well as historical temperature and PDSI data. While full durations of dendrochronologies are indicated in the stacked barplot in Fig. 4, Fig. 3 shows data series only for the time frame since 1901, when a significant number of tree chronologies in each local area as well as climate variability data are available. Fig. 4 shows that in the wetland area, the trees are characterized by longevity, with several chronologies dating back to the 1780s–1800s, several decades beyond the longest chronologies in the dry land area.

Figs. 3 and 4 also indicate that in the dry area, a large fraction of trees emerged between the 1930s and 1950s, which corresponds to the two major bursts in the TRW data when considerable fractions of young trees were included in the statistics, leading to considerable non-stationarity of the average TRW curve. We believe that these bursts indicate the replacement of older trees by new ones, which in turn could be enforced by the loss of a significant fraction of trees during two major climate extremes: a prolonged drought in the early 1930s characterized by a near 10-year decline in PDSI with culmination in 1936 (accompanied by several hot weather anomalies), and a major winter temperature anomaly in 1941–1942 (with night temperatures registered at the local meteo station going below -45^{o}C in late January) [61], the latter resulting in three- to ten-fold growth suppression in the majority of the survived trees in the same year. Remarkably, no similarly pronounced effect could be observed for the trees located within the peat bog area. For a more relevant comparison, separate curves for the TRW data for chronologies starting before 1930 and 1940, indicate that in the following years they exhibit similar variability patterns like the overall average in this dry area and thus likely demonstrate similar cross-correlation patterns with hydroclimatic variation data (shown in the middle and lower panels of Fig. 3).

3.3. Detrended fluctuation analysis

Fig. 5 shows that for the TRW data, the consensus estimates of the Hurst exponent from the results obtained by all three methods are $H \cong 1.0$. The histogram shows the distribution of the estimates from individual TRW data series obtained separately for each tree from the least-mean-square algebraic fits of the fluctuation functions $F(s) \propto s^{H}$. Because of different durations of dendrochronologies, the fitting range was restricted to $s = 5 \dots 33$. For the temperature records, all methods show asymptotic slopes H between 0.6 and 0.7. Regarding the PDSI, at small scales, the Hurst exponent is close to one, likely reflecting additional short-term memory corresponding to the accumulation of drought effects, although the asymptotic slopes are in the same range as for the temperature data.

3.4. Detrended cross-correlation analysis

We analyzed cross-correlations between individual dendrochronological data series using both the conventional cross-correlation coefficient matrix and the multi-scale cross-correlation coefficients obtained by D(P)CCA with CMA- and DFA-based detrending calculated for scales $s = 2^{k} + 1$, where $k = 1, 2, \dots, 5$. Figure S3 shows that at all scales, the highest positive cross-correlations were observed for the trees located within the areas with minimum and maximum elevations, in the lowest area in the eastern part of the peat bog, and in the elevated dry land area west of the peat bog. However, only a weak negative correlation tendency could be observed between these areas.

Figs. 6 and 7 show cross-correlations between individual dendrochronological data series and local temperature variations within the 5-year time window up to the end of the growth period for the year of interest (from September to August). The results indicate that TRW is negatively correlated with spring and summer temperatures and positively correlated with the Palmer drought severity index (PDSI) in the same year. For the elevated dry land area around the peat bog, the above effect extends to interannual scales, indicating that prolonged heatwaves and associated droughts are among the factors limiting tree growth. In marked contrast, in

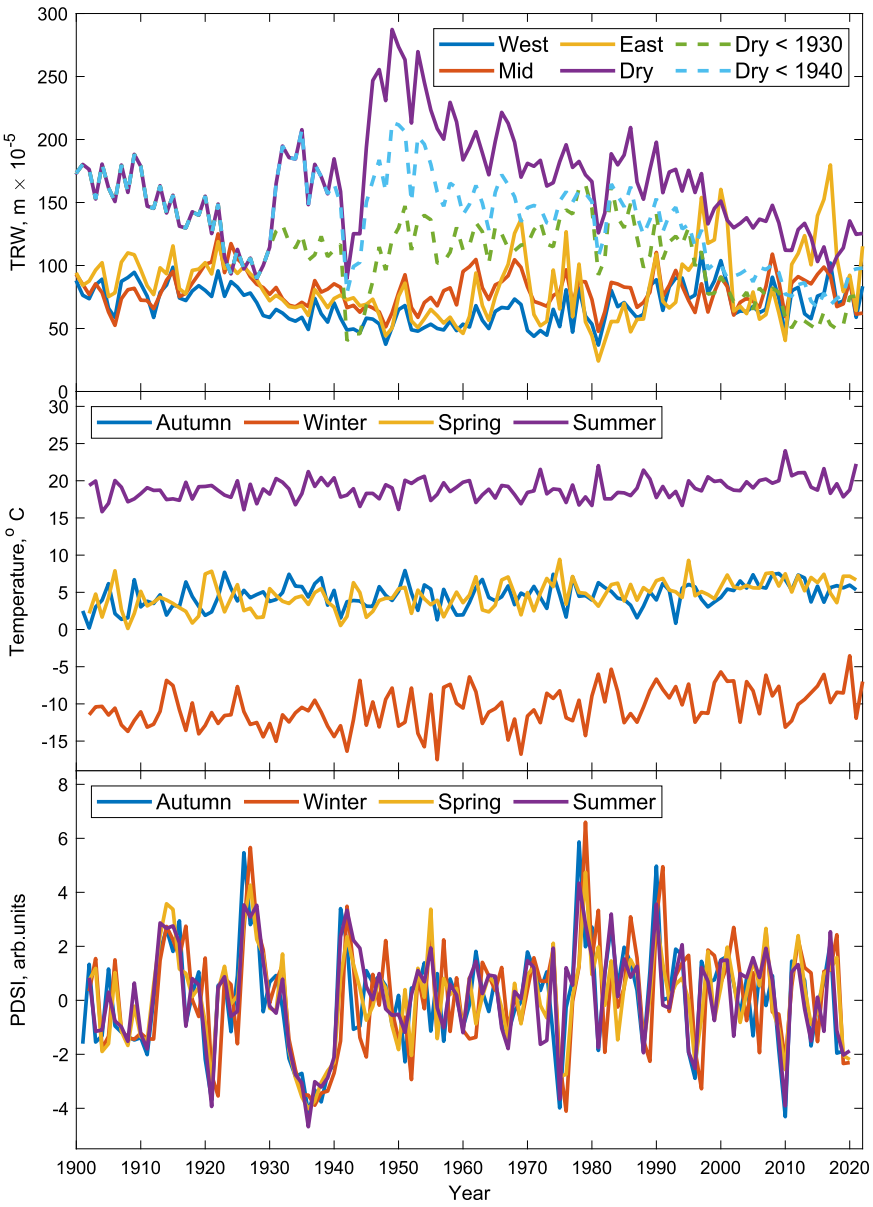

Fig. 3. TRW data were averaged over three locations in the peat bog area, altogether $n = 100$ data series, as well as averaged data over $n = 40$ data series from three dry land locations at local elevations surrounding the peat bog area (upper panel). Since in the dry area a large fraction of trees emerged between the 1930s and 1950s, dashed curves additionally show data for chronologies starting < 1930 and < 1940, respectively. Seasonal average temperature (middle panel) and PDSI (lower panel) variations.

the waterlogged peat bog area, a reversed tendency could be observed, with prolonged dry periods as well as warmer springs and summers over several consecutive years leading to increasing tree growth with a one- to three-year time lag.

However, one can notice that the long-term negative correlations between TRW and temperature variations for the elevated dry land area only become stronger with increasing scale. Thus, they could be potentially attributed to the long-term increase in temperatures associated with climate change, eventually coinciding with the overall reduction of the tree growth rate in this area. Remarkably, a reminiscent pattern was observed around 100 years ago. Thus, these correlations could be at least in part attributed to the aging effects of the trees (see Fig. 3). Since in all cases the respective trends could be in the first approximation represented by their linear fits, we next repeat a similar analysis using DFA with linear detrending. Figure S4 shows that in the modified DPCCA results, these previously pronounced negative correlations have been considerably reduced and remain notable only for the spring temperatures. Figure S5 also shows that, while the absolute values of cross-correlation coefficients were reduced after linear detrending, the contrast between correlation patterns in the lowest area in the eastern part of the peat bog and the surrounding dry land was enhanced.

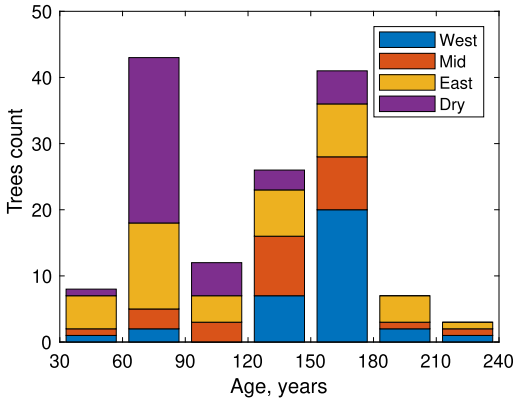

Fig. 4. Stacked barplot representing the distribution of dendrochronological durations (tree ages) for each of the studied locations.

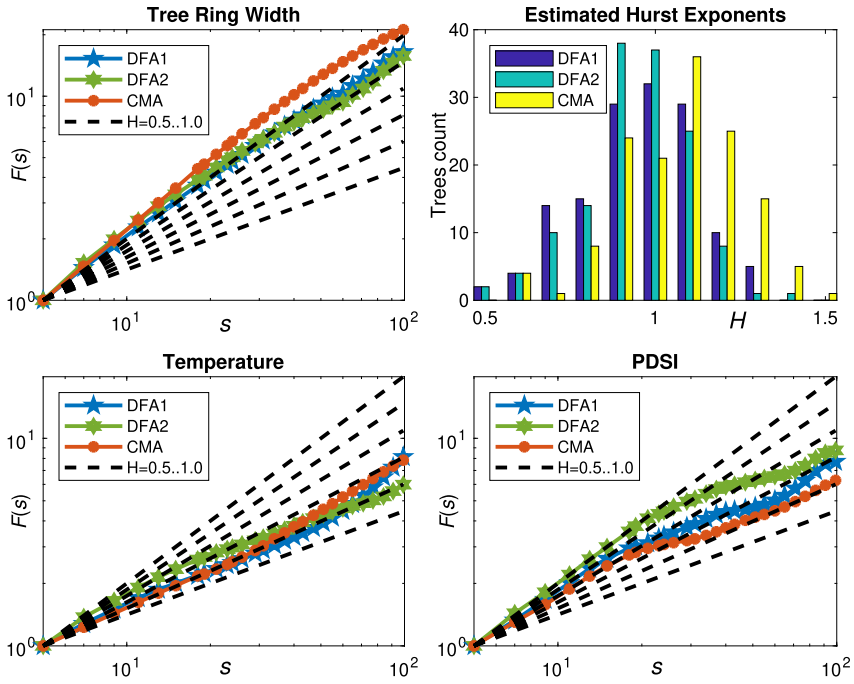

Fig. 5. Fluctuation functions for TRW, temperature, and PDSI data variations were obtained by first- and second-order DFA methods, as well as by CMA detrended fluctuation analysis methods. Dashed lines show theoretical slopes corresponding to linearly long-term correlated (fractional Gaussian noise) data series $F(s) \propto s^H$, from the simplest case $H = 0.5$ (corresponding to uncorrelated "while noise" data) to $H = 1.0$ (corresponding to the upper bound for stationary data). Histograms show the estimated Hurst exponents H for the scales between $s = 5 \ldots 33$.

Figs. 8 and 9 show that the long-term negative correlations between TRW and temperature variations for the elevated dry land area are largely eliminated from the partial correlations between the same variables when tree age is considered as a separate contributing variable in the model. This indicates that they could be attributed to the coincidence between tree aging and climate warming. In contrast, negative cross-correlations between TRW and PDSI for the wet area exhibited qualitatively similar patterns for all three variants of detrending.

4. Discussion, conclusion, and outlook

Despite recent evidence that *Pinus* are among the few species in the boreal ecosystem that respond favorably to increasing temperatures [6], they are particularly sensitive to prolonged droughts, and thus temperature effects likely play a secondary role, with warming promoting better growth only under non-drought conditions [62,63]. Sufficient water resources play a major role in the welfare of the forest ecosystem. From a hydrometeorological perspective, increased temperatures promote the intensification of drought conditions by increasing evapotranspiration. Thus, increased precipitation is required to counterbalance and prevent the development of drought conditions. On a local scale, water may come from alternative resources such as groundwater and/or accumulate in waterlogged peatlands. Accordingly, along with global and regional climate drivers, local hydrological conditions

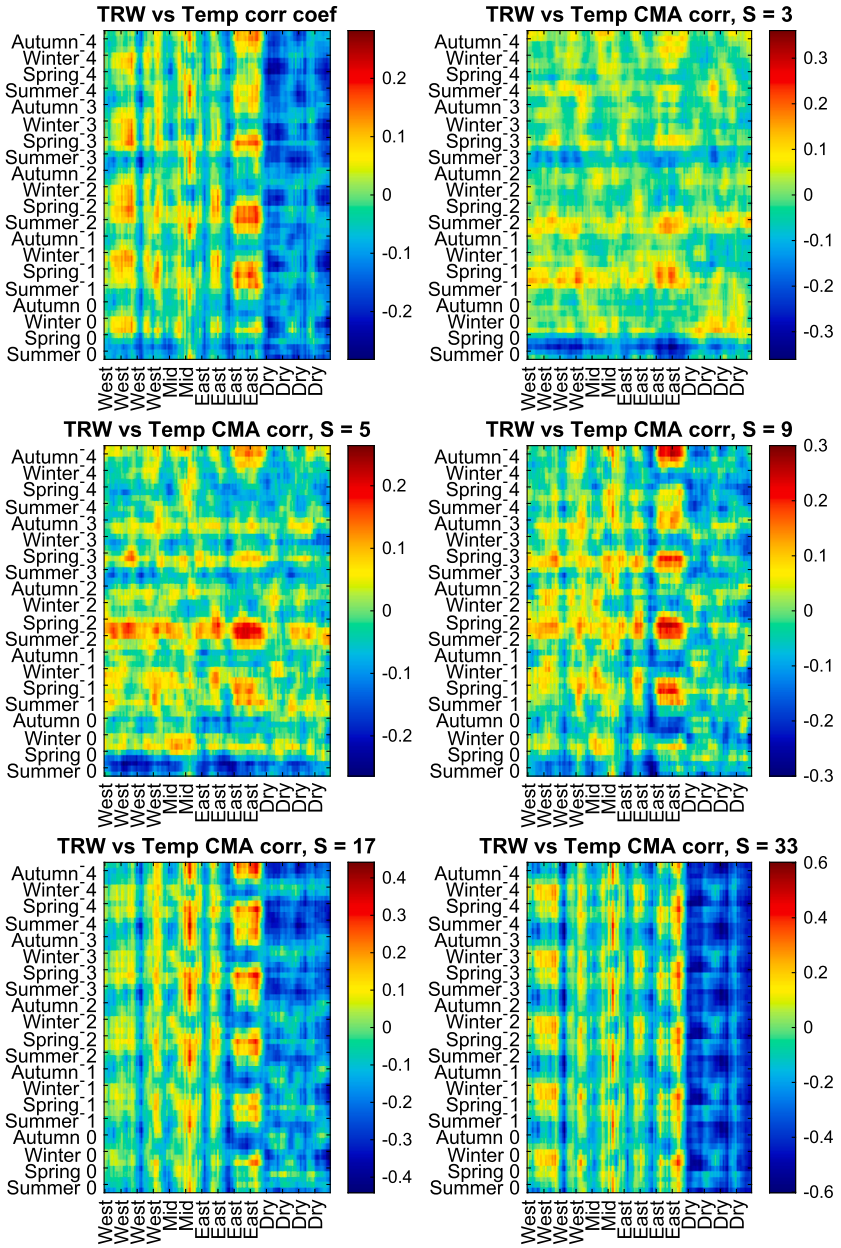

Fig. 6. Multi-scale conventional and DPCCA (with CMA-based detrending) cross-correlation coefficients between individual TRW data series, altogether for $n = 140$ trees growing in different parts of the bog ($n = 32$ in the western, $n = 26$ in the central, $n = 42$ in the eastern), as well as in the surrounding elevated dry land area ($n = 40$ altogether in three surrounding locations), and the local temperature variations over five years prior and during the growth period for a given year (September to August). Monthly resolution data were analyzed; however, for noise reduction and better visibility, they are displayed with seasonal resolution obtained by moving average in a 3×3 window over the entire heatmap.

are among the key factors that determine stress resilience and are essential for the preservation of boreal ecosystems in a changing climate [64,65]. Our results indicate that the climate stress response in dry land and waterlogged peat bog areas exhibits considerably contrasting patterns, with reversed correlations with temperature and PDSI variations.

In particular, while trees in elevated dry land areas are generally characterized by higher growth rates, this comes at the cost of considerably reduced drought stress resilience. In addition, more pronounced growth reduction with aging as well as more frequent replacement of the trees by new ones, likely following significant losses of trees to climate extremes, could be observed (see Fig. 3). In contrast, while exhibiting lower productivity, the forest ecosystem in the wetland area is characterized by longevity, with several chronologies dating back to the 1780s–1800s, several decades beyond the longest chronologies in the dry land area (see Fig. 4). It also appears considerably less sensitive to heat and associated drought stress and demonstrates considerably weaker aging trends (see Fig. 3).

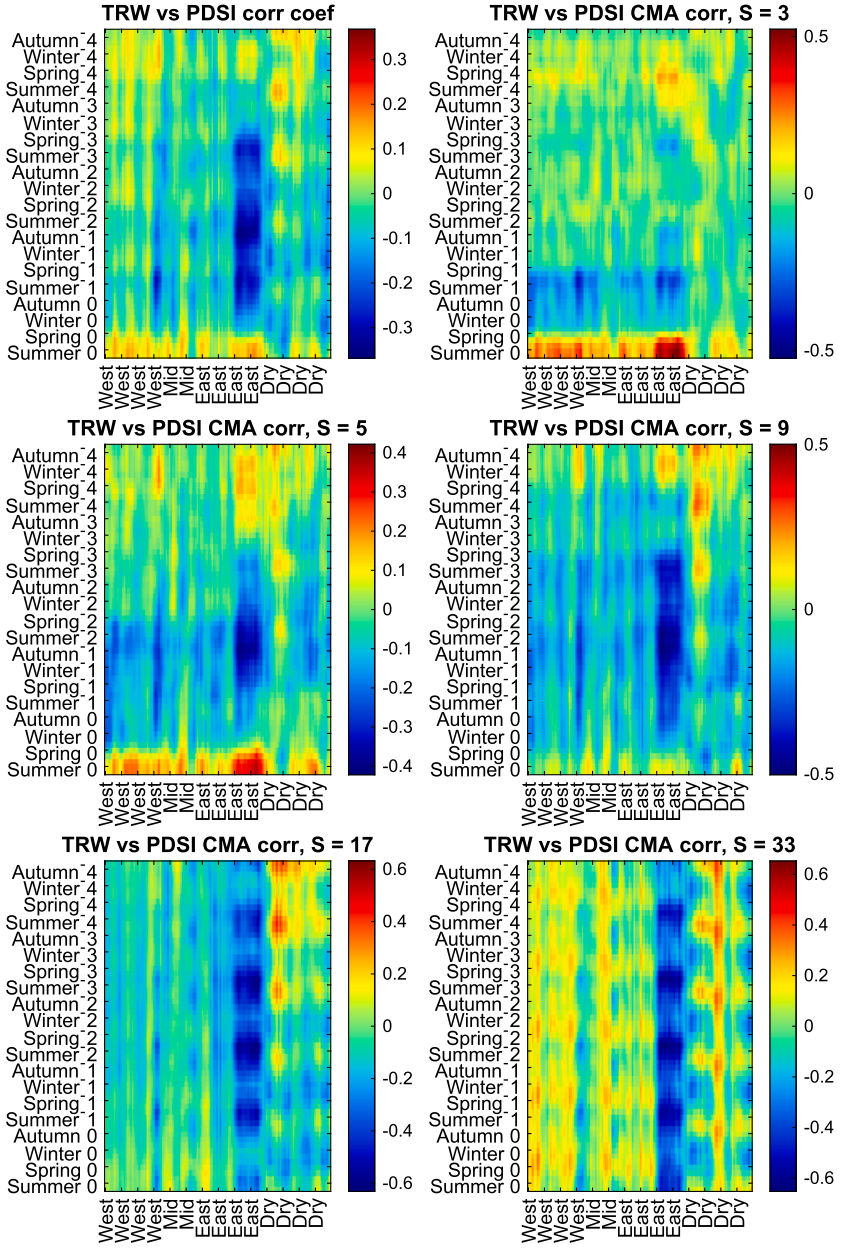

Fig. 7. Multi-scale conventional and DPCCA (with CMA-based detrending) cross-correlation coefficients between individual TRW data series, altogether for $n = 140$ trees growing in different parts of the bog ($n = 32$ in the western, $n = 26$ in the central, $n = 42$ in the eastern), as well as in the surrounding elevated dry land area ($n = 40$ altogether in three surrounding locations), and the local PDSI variations over five years prior and during the growth period for a given year (September to August). Monthly resolution data were analyzed; however, for noise reduction and better visibility, they are displayed with seasonal resolution obtained by moving average in a 3×3 window over the entire heatmap.

From a methodological perspective, both TRW and hydroclimatic data series exhibit long-term memory. The histogram in Fig. 5 indicates that H values are slightly underestimated by DFA and slightly overestimated by CMA compared with the consensus value $H \cong 1.0$, which could be attributed to the earlier onset of finite size effects in higher-order detrending methods (for additional methodological details, we refer to [58,28,66,59] and references therein). We like to note that this consensus value is in agreement with the results for tree-ring data reported in the recent literature [33,34,57]. Similarly, the results for hydroclimatic time series are also in agreement with earlier studies ($H \cong 0.65$ appeared to be the most commonly observed exponent for long-term temperature observations, according to literature data [28,66,59]. Regarding the PDSI, at small scales, the Hurst exponent is close to one, likely reflecting additional short-term memory corresponding to the accumulation of the drought effects. Although the asymptotic slopes are likely in the same range as for the temperature data, they appear in between the typical exponents for the (non-accumulated) precipitation and (accumulated) river runoff data [67,68] (for a recent review, see also [69] and references therein).

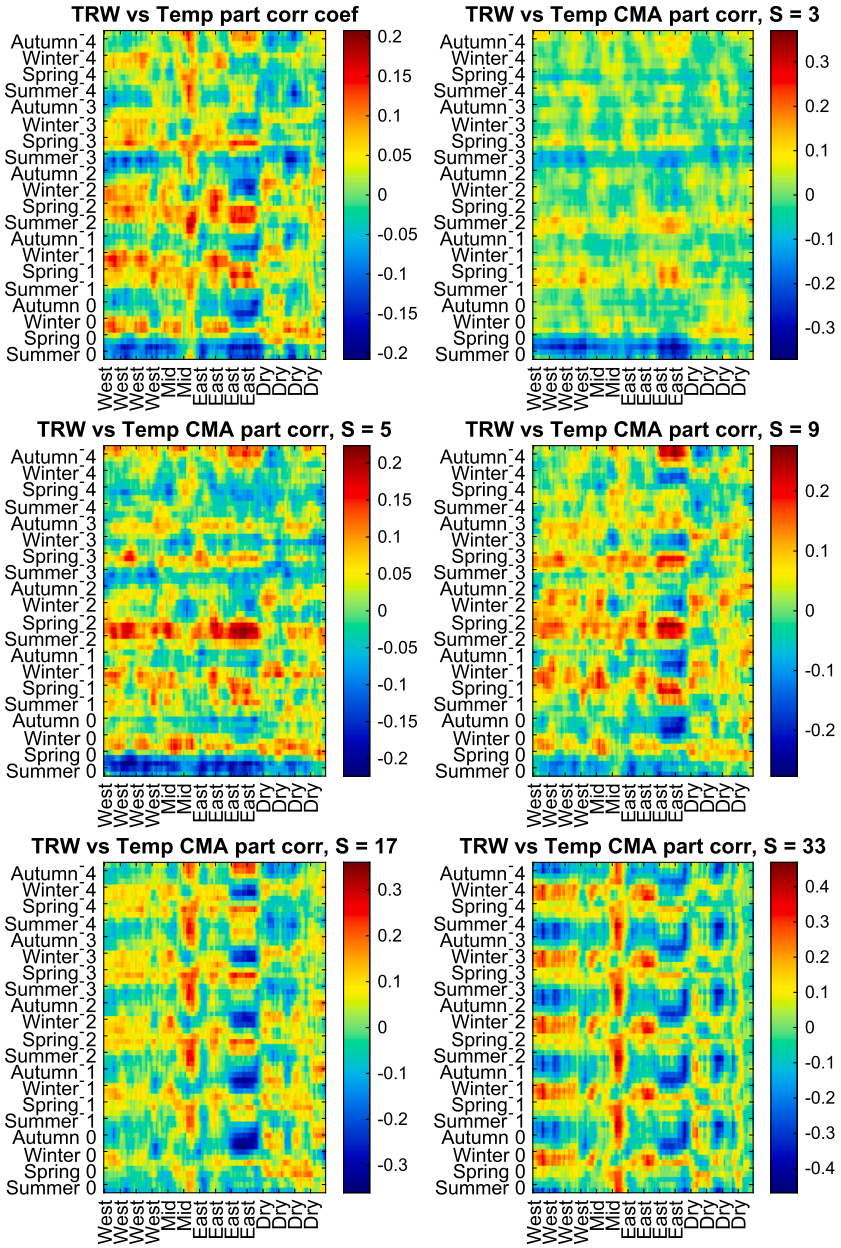

Fig. 8. Multi-scale conventional and DPCCA (with CMA-based detrending) partial cross-correlation coefficients between individual TRW data series, altogether for $n = 141$ trees growing in different parts of the bog ($n = 33$ in the western, $n = 26$ in the central, $n = 42$ in the eastern), as well as in the surrounding elevated dry land area ($n = 40$ altogether in three surrounding locations), and the local temperature variations over five years prior and during the growth period for a given year (September to August). Monthly resolution data were analyzed; however, for noise reduction and better visibility, they are displayed with seasonal resolution obtained by moving average in a 3×3 window over the entire heatmap.

While the presence of long-term memory indicates that detrending methods are more appropriate than conventional time series analysis tools, the selection of particular detrending methods is often based on the balance between their performance and the interpretability of the results. Second-order detrending in the cumulative data series ("profile") became widespread largely because of its ability to fit fragments of periodic oscillations, which is especially relevant when analyzing high-resolution data (daily, weekly, and monthly) on interannual scales. Notably, second-order detrending in the profile has been recently and successfully applied to long-term annual TRW data in several dendrochronological studies [33,34,57]. On the other hand, simple linear effects are easier to interpret than more complex nonlinear interactions. In this aspect, cross-correlation analysis after CMA-based detrending provides clearly interpretable relationships between downward and upward interannual trends in the TRW and hydroclimatic data series, respectively (see Fig. 2). The duration of the trends, time lags characterizing delayed effects, and strength of the relations characterized by the cross-correlation coefficients are the only parameters produced by this analysis, and all of them could be easily

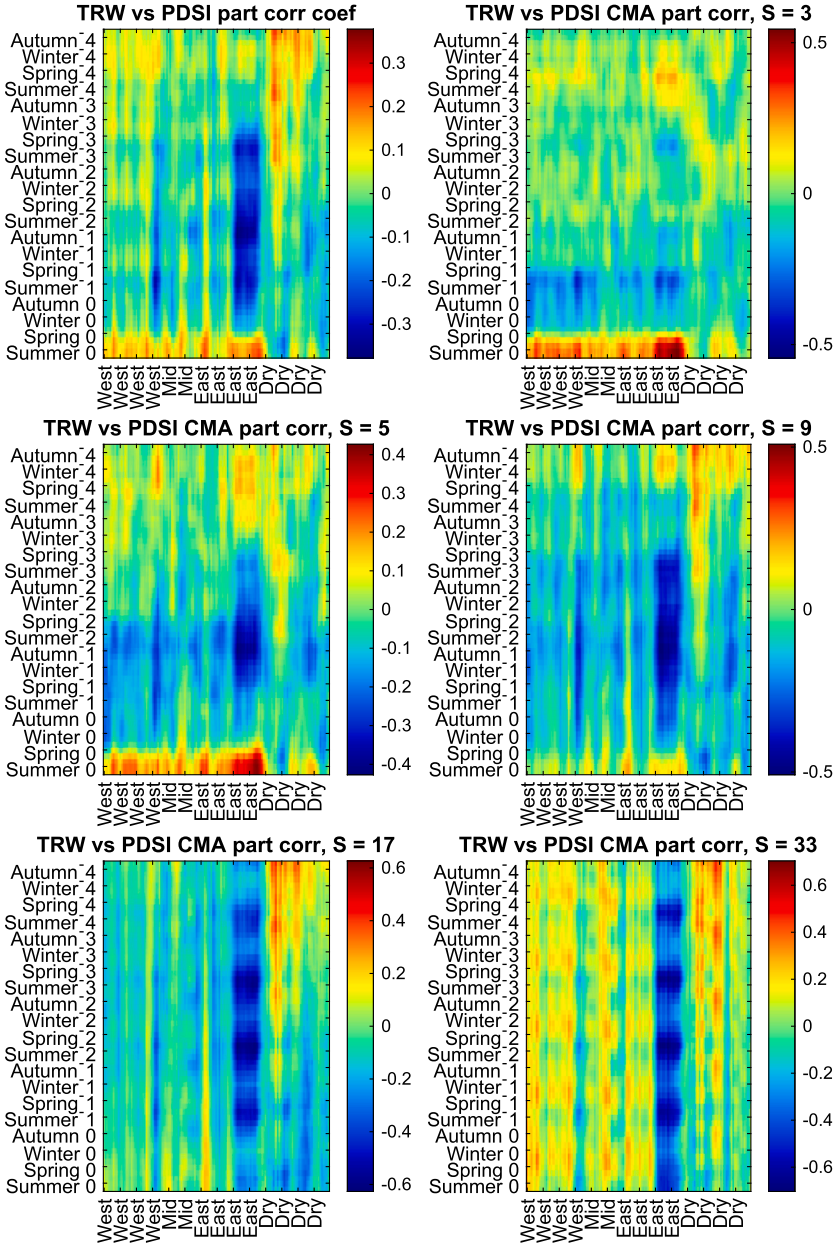

Fig. 9. Multi-scale conventional and DPCCA (with CMA-based detrending) partial cross-correlation coefficients between individual TRW data series, altogether for $n = 141$ trees growing in different parts of the bog ($n = 33$ in the western, $n = 26$ in the central, $n = 42$ in the eastern), as well as in the surrounding elevated dry land area ($n = 40$ altogether in three surrounding locations), and the local PDSI variations over five years prior and during the growth period for a given year (September to August). Monthly resolution data were analyzed; however, for noise reduction and better visibility, they are displayed with seasonal resolution obtained by moving average in a 3×3 window over the entire heatmap.

interpreted by a domain expert in a non-mathematically focused field. Moreover, nonlinear interactions observed in complex systems often are the result of several superimposed effects that cannot be attributed to a single origin. In this context, partial correlation analysis is capable of providing additional insights into the complex interplay of effects leading to their attribution to their respective origins and thus could be recommended for a better understanding of the results obtained by nonlinear methods.

For the development and accumulation of drought conditions in the forest ecosystem, not only the absolute temperature and precipitation levels but also their timings and durations are crucial factors. Long-term correlations of the hydroclimatic variables are associated with clustering of anomalies [22,70,23], as well as prolonged droughts [28,71,67] that are drastically underestimated by seemingly established mathematical methods (see, e.g., [72,73,68,59] and references therein). While conventional correlation analysis provides an overall characterization of the response to climate variations, detrended multi-scaled analysis methods hold the key to a better understanding of the contribution of clustered, prolonged, and delayed effects [24–26].

While tree-ring data are negatively correlated with spring and summer temperatures and positively correlated with PDSI in the same year, indicating that heatwaves and droughts represent the limiting factors, at interannual scales, remarkable contrasts can be observed between areas with different local hydrological conditions. In particular, for the peat bog area, positive TRW trends over several consecutive years tend to follow negative PDSI trends and positive spring and summer temperature trends of the same duration with a time lag between one and three years, indicating that prolonged dry periods as well as warmer springs and summers appear beneficial for the increased annual growth. In contrast, for the surrounding elevated dry land area, a reverse tendency can be observed, with pronounced negative long-term correlations with temperature and positive correlations with PDSI. Our results indicate that prolonged dry periods with warm springs and summers over several consecutive years, with most pronounced effects observed for 5- and 9-year durations, improved the tree growth in the wetland area, typically with a 1–3 year time lag. This indicates that the preservation of waterlogged areas could be key to the survival of boreal ecosystems in extreme climate conditions, including prolonged droughts, as long as the water supply remains sufficient.

Although dendrochronological data series remain the only long-term data source characterizing the local ecosystem in our study, indicating an obvious limitation, we believe they could be complemented by additional sources. Multi-year vegetation indices can be extracted from satellite-based multispectral observations, at least for recent decades, providing potentially complementary information about long-term correlations in vegetation dynamics as well as multi-scale cross-correlations with hydroclimatic indicators.

Nevertheless, the considered methodological modifications would be helpful in revealing the complex interconnections between global, regional, and local factors to unravel and characterize in a quantitative manner the keynote factors governing stress resilience. In turn, using adequate models that consider long-term auto- and cross-correlations in the data would improve reliability, eventually facilitating improved risk assessment for the boreal ecosystems and thus leading to better environmental management planning.

CRediT authorship contribution statement

Mikhail I. Bogachev: Conceptualization, Data curation, Investigation, Methodology, Software, Supervision, Validation, Visualization, Writing – original draft, Writing – review & editing. **Artur M. Gafurov:** Investigation, Resources. **Pavel Y. Iskandirov:** Investigation. **Dmitrii I. Kaplun:** Supervision. **Airat R. Kayumov:** Conceptualization, Methodology, Writing – original draft, Writing – review & editing. **Asya I. Lyanova:** Investigation. **Nikita S. Pyko:** Formal analysis, Investigation, Methodology. **Svetlana A. Pyko:** Formal analysis, Investigation, Methodology. **Anastasiia N. Safonova:** Funding acquisition, Project administration. **Aleksandr M. Sinitca:** Methodology, Software. **Bulat M. Usmanov:** Investigation, Resources. **Denis V. Tishin:** Conceptualization, Data curation, Investigation, Methodology, Resources, Supervision, Validation, Visualization, Writing – original draft, Writing – review & editing.

Declaration of competing interest

The authors declare that they have no known competing financial interests or personal relationships that could have appeared to influence the work reported in this paper.

Data availability

Data will be made available on request.

Acknowledgements

The authors would like to acknowledge the financial support of this research by the Russian Science Foundation (grant No. 22-76-10042), https://rscf.ru/en/project/22-76-10042/.

Appendix A. Supplementary material

Supplementary material related to this article can be found online at https://doi.org/10.1016/j.heliyon.2023.e21574.

References

[1] P.M. Della-Marta, M.R. Haylock, J. Luterbacher, H. Wanner, Doubled length of western European summer heat waves since 1880, J. Geophys. Res. 112 (D15) (2007).
[2] D. Barriopedro, E.M. Fischer, J. Luterbacher, R.M. Trigo, R. García-Herrera, The hot summer of 2010: redrawing the temperature record map of Europe, Science 332 (6026) (2011) 220–224.
[3] X. Yuan, Y. Wang, P. Ji, P. Wu, J. Sheffield, J.A. Otkin, A global transition to flash droughts under climate change, Science 380 (6641) (2023) 187–191.
[4] J. Zscheischler, S. Westra, B.J. Van Den Hurk, S.I. Seneviratne, P.J. Ward, A. Pitman, A. AghaKouchak, D.N. Bresch, M. Leonard, T. Wahl, et al., Future climate risk from compound events, Nat. Clim. Change 8 (6) (2018) 469–477.
[5] R. Teskey, T. Wertin, I. Bauweraerts, M. Ameye, M.A. McGuire, K. Steppe, Responses of tree species to heat waves and extreme heat events, Plant Cell Environ. 38 (9) (2015) 1699–1712.
[6] J.D. Birch, J.A. Lutz, E. Hogg, S.W. Simard, R. Pelletier, G.H. LaRoi, J. Karst, Decline of an ecotone forest: 50 years of demography in the southern boreal forest, Ecosphere 10 (4) (2019) e02698.
[7] P. Evans, C.D. Brown, The boreal–temperate forest ecotone response to climate change, Environ. Rev. 25 (4) (2017) 423–431.
[8] L. Matías, A.S. Jump, Interactions between growth, demography and biotic interactions in determining species range limits in a warming world: the case of pinus sylvestris, For. Ecol. Manag. 282 (2012) 10–22.

[9] V. Matskovsky, Climatic signal in tree-ring width chronologies of conifers in European Russia, Int. J. Climatol. 36 (9) (2016) 3398–3406.
[10] E.R. Cook, O. Solomina, V. Matskovsky, B.I. Cook, L. Agafonov, A. Berdnikova, E. Dolgova, A. Karpukhin, N. Knysh, M. Kulakova, et al., The European Russia drought atlas (1400–2016 ce), Clim. Dyn. 54 (2020) 2317–2335.
[11] A.J. Soja, N.M. Tchebakova, N.H. French, M.D. Flannigan, H.H. Shugart, B.J. Stocks, A.I. Sukhinin, E. Parfenova, F.S. Chapin III, P.W. Stackhouse Jr, Climate-induced boreal forest change: predictions versus current observations, Glob. Planet. Change 56 (3–4) (2007) 274–296.
[12] C.D. Allen, A.K. Macalady, H. Chenchouni, D. Bachelet, N. McDowell, M. Vennetier, T. Kitzberger, A. Rigling, D.D. Breshears, E.T. Hogg, et al., A global overview of drought and heat-induced tree mortality reveals emerging climate change risks for forests, For. Ecol. Manag. 259 (4) (2010) 660–684.
[13] M. Scheffer, M. Hirota, M. Holmgren, E.H. Van Nes, F.S. Chapin III, Thresholds for boreal biome transitions, Proc. Natl. Acad. Sci. 109 (52) (2012) 21384–21389.
[14] L.E. Frelich, P.B. Reich, Will environmental changes reinforce the impact of global warming on the prairie–forest border of central North America?, Front. Ecol. Environ. 8 (7) (2010) 371–378.
[15] A. Rigling, P.O. Waldner, T. Forster, O.U. Bräker, A. Pouttu, Ecological interpretation of tree-ring width and intraannual density fluctuations in pinus sylvestris on dry sites in the central Alps and Siberia, Can. J. For. Res. 31 (1) (2001) 18–31.
[16] E.A. Vaganov, M.K. Hughes, A.V. Shashkin, Growth Dynamics of Conifer Tree Rings: Images of Past and Future Environments, vol. 183, Springer Science & Business Media, 2006.
[17] A.E. Bozkurt, E.A. Şahan, N. Köse, Growth responses of pinus sylvestris l. to climate from the southeastern limit of its natural distribution area, Turkey, Dendrochronologia 70 (2021) 125897.
[18] I.E. Zlobin, Linking the growth patterns of coniferous species with their performance under climate aridization, Sci. Total Environ. 831 (2022) 154971.
[19] R.L. Salomón, R.L. Peters, R. Zweifel, U.G. Sass-Klaassen, A.I. Stegehuis, M. Smiljanic, R. Poyatos, F. Babst, E. Cienciala, P. Fonti, et al., The 2018 European heatwave led to stem dehydration but not to consistent growth reductions in forests, Nat. Commun. 13 (1) (2022) 1–11.
[20] M. Vlam, P. Van der Sleen, P. Groenendijk, P.A. Zuidema, Tree age distributions reveal large-scale disturbance-recovery cycles in three tropical forests, Front. Plant Sci. 7 (2017) 1984.
[21] V. Čada, V. Trotsiuk, P. Janda, M. Mikoláš, R. Bače, T.A. Nagel, R.C. Morrissey, A.J. Tepley, O. Vostarek, K. Begović, et al., Quantifying natural disturbances using a large-scale dendrochronological reconstruction to guide forest management, Ecol. Appl. 30 (8) (2020) e02189.
[22] E. Koscielny-Bunde, A. Bunde, S. Havlin, H.E. Roman, Y. Goldreich, H.-J. Schellnhuber, Indication of a universal persistence law governing atmospheric variability, Phys. Rev. Lett. 81 (3) (1998) 729.
[23] A. Bunde, J.F. Eichner, J.W. Kantelhardt, S. Havlin, Long-term memory: a natural mechanism for the clustering of extreme events and anomalous residual times in climate records, Phys. Rev. Lett. 94 (4) (2005) 048701.
[24] A. Bunde, U. Büntgen, J. Ludescher, J. Luterbacher, H. Von Storch, Is there memory in precipitation?, Nat. Clim. Change 3 (3) (2013) 174–175.
[25] A. Bunde, J. Ludescher, C.L. Franzke, U. Büntgen, How significant is West Antarctic warming?, Nat. Geosci. 7 (4) (2014) 246–247.
[26] J. Ludescher, A. Bunde, C.L. Franzke, H.J. Schellnhuber, Long-term persistence enhances uncertainty about anthropogenic warming of Antarctica, Clim. Dyn. 46 (2016) 263–271.
[27] C.-K. Peng, S.V. Buldyrev, S. Havlin, M. Simons, H.E. Stanley, A.L. Goldberger, Mosaic organization of dna nucleotides, Phys. Rev. E 49 (2) (1994) 1685.
[28] J.F. Eichner, E. Koscielny-Bunde, A. Bunde, S. Havlin, H.-J. Schellnhuber, Power-law persistence and trends in the atmosphere: a detailed study of long temperature records, Phys. Rev. E 68 (4) (2003) 046133.
[29] J. Ludescher, M.I. Bogachev, J.W. Kantelhardt, A.Y. Schumann, A. Bunde, On spurious and corrupted multifractality: the effects of additive noise, short-term memory and periodic trends, Phys. A, Stat. Mech. Appl. 390 (13) (2011) 2480–2490.
[30] J. Ludescher, A. Bunde, H.J. Schellnhuber, Statistical significance of seasonal warming/cooling trends, Proc. Natl. Acad. Sci. 114 (15) (2017) E2998–E3003.
[31] N. Yuan, M. Ding, J. Ludescher, A. Bunde, Increase of the Antarctic sea ice extent is highly significant only in the Ross sea, Sci. Rep. 7 (1) (2017) 1–8.
[32] J. Ludescher, N. Yuan, A. Bunde, Detecting the statistical significance of the trends in the Antarctic sea ice extent: an indication for a turning point, Clim. Dyn. 53 (2019) 237–244.
[33] J. Ludescher, A. Bunde, U. Büntgen, H.J. Schellnhuber, Setting the tree-ring record straight, Clim. Dyn. 55 (11) (2020) 3017–3024.
[34] U. Büntgen, D. Arseneault, É. Boucher, O.V. Churakova, F. Gennaretti, A. Crivellaro, M.K. Hughes, A.V. Kirdyanov, L. Klippel, P.J. Krusic, et al., Prominent role of volcanism in common era climate variability and human history, Dendrochronologia 64 (2020) 125757.
[35] U. Büntgen, D. Arseneault, É. Boucher, O.V. Churakova, F. Gennaretti, A. Crivellaro, M.K. Hughes, A.V. Kirdyanov, L. Klippel, P.J. Krusic, et al., Recognising bias in common era temperature reconstructions, Dendrochronologia 74 (2022) 125982.
[36] B. Podobnik, H.E. Stanley, Detrended cross-correlation analysis: a new method for analyzing two nonstationary time series, Phys. Rev. Lett. 100 (8) (2008) 084102.
[37] N. Yuan, Z. Fu, H. Zhang, L. Piao, E. Xoplaki, J. Luterbacher, Detrended partial-cross-correlation analysis: a new method for analyzing correlations in complex system, Sci. Rep. 5 (1) (2015) 1–7.
[38] J. Alvarez-Ramirez, E. Rodriguez, J.C. Echeverría, Detrending fluctuation analysis based on moving average filtering, Phys. A, Stat. Mech. Appl. 354 (2005) 199–219.
[39] D.M. Olson, E. Dinerstein, E.D. Wikramanayake, N.D. Burgess, G.V. Powell, E.C. Underwood, J.A. D'amico, I. Itoua, H.E. Strand, J.C. Morrison, et al., Terrestrial ecoregions of the world: a new map of life on eartha new global map of terrestrial ecoregions provides an innovative tool for conserving biodiversity, Bioscience 51 (11) (2001) 933–938.
[40] Volzhsko-Kamsky State Natural Biosphere Reserve, https://vkgz.ru/en/, https://en.unesco.org/biosphere/eu-na/great-volzhsko-kamsky/. (Accessed 8 October 2023).
[41] O.V. Bakin, T.V. Rogova, A.P. Sitnikov, Vascular Plants of the Republic of Tatarstan, Kazan University Press, 2000.
[42] E.R. Cook, L.A. Kairiukstis, Methods of Dendrochronology: Applications in the Environmental Sciences, Springer Science & Business Media, 2013.
[43] F. Rinn, Tsap-Win: Time Series Analysis and Presentation for Dendrochronology and Related Applications, Frank Rinn, Heidelberg, 2003.
[44] H.D. Grissino-Mayer, Evaluating crossdating accuracy: a manual and tutorial for the computer program cofecha, 2001.
[45] V.N. Razuvaev, O.N. Bulygina, Baseline climatological data sets for eastern Europe area, in: Regional Aspects of Climate-Terrestrial-Hydrologic Interactions in Non-boreal Eastern Europe, Springer, 2009, pp. 17–22.
[46] G. van der Schrier, J. Barichivich, K. Briffa, P. Jones, A scpdsi-based global data set of dry and wet spells for 1901–2009, J. Geophys. Res. 118 (10) (2013) 4025–4048.
[47] J. Barichivich, T. Osborn, I. Harris, G. van der Schrier, P. Jones, Monitoring global drought using the self-calibrating palmer drought severity index, [in: dunn rjh, aldred f, gobron n, miller jb and willett km (Eds.), State of the Climate in 2020], Bull. Am. Meteorol. Soc. 102 (8) (2021) S68–S70.
[48] C.J. Tucker, Red and photographic infrared linear combinations for monitoring vegetation, Remote Sens. Environ. 8 (2) (1979) 127–150.
[49] G. Rondeaux, M. Steven, F. Baret, Optimization of soil-adjusted vegetation indices, Remote Sens. Environ. 55 (2) (1996) 95–107.
[50] Z. Jiang, A.R. Huete, K. Didan, T. Miura, Development of a two-band enhanced vegetation index without a blue band, Remote Sens. Environ. 112 (10) (2008) 3833–3845.
[51] A.A. Gitelson, M.N. Merzlyak, Remote sensing of chlorophyll concentration in higher plant leaves, Adv. Space Res. 22 (5) (1998) 689–692.
[52] C. Schuster, M. Förster, B. Kleinschmit, Testing the red edge channel for improving land-use classifications based on high-resolution multi-spectral satellite data, Int. J. Remote Sens. 33 (17) (2012) 5583–5599.
[53] J. Weier, D. Herring, Measuring vegetation (ndvi & evi), NASA Earth Obs. 20 (2000) 2.

[54] S. Candiago, F. Remondino, M. De Giglio, M. Dubbini, M. Gattelli, Evaluating multispectral images and vegetation indices for precision farming applications from uav images, Remote Sens. 7 (4) (2015) 4026–4047.
[55] S. Huang, L. Tang, J.P. Hupy, Y. Wang, G. Shao, A commentary review on the use of normalized difference vegetation index (ndvi) in the era of popular remote sensing, J. For. Res. 32 (1) (2021) 1–6.
[56] S.K. McFeeters, The use of the normalized difference water index (ndwi) in the delineation of open water features, Int. J. Remote Sens. 17 (7) (1996) 1425–1432.
[57] U. Büntgen, K. Allen, K.J. Anchukaitis, D. Arseneault, É. Boucher, A. Bräuning, S. Chatterjee, P. Cherubini, C. Corona, F. Gennaretti, et al., The influence of decision-making in tree ring-based climate reconstructions, Nat. Commun. 12 (1) (2021) 1–10.
[58] J.W. Kantelhardt, E. Koscielny-Bunde, H.H. Rego, S. Havlin, A. Bunde, Detecting long-range correlations with detrended fluctuation analysis, Phys. A, Stat. Mech. Appl. 295 (3–4) (2001) 441–454.
[59] M.I. Bogachev, N. Yuan, A. Bunde, Fractals and multifractals in geophysical time series, in: Fractals, CRC Press, 2017, pp. 231–271.
[60] M. Bogachev, A. Sinitca, K. Grigarevichius, N. Pyko, A. Lyanova, M. Tsygankova, E. Davletshin, K. Petrov, T. Ageeva, S. Pyko, D. Kaplun, A. Kayumov, Y. Mukhamedshina, Video-based marker-free tracking and multi-scale analysis of mouse locomotor activity and behavioral aspects in an open field arena: a perspective approach to the quantification of complex gait disturbances associated with Alzheimer's disease, Front. Neuroinform. 17 (2023) 1101112.
[61] S. Brönnimann, J. Luterbacher, J. Staehelin, T. Svendby, G. Hansen, T. Svenøe, Extreme climate of the global troposphere and stratosphere in 1940–42 related to el niño, Nature 431 (7011) (2004) 971–974.
[62] J.R. Brooks, L.B. Flanagan, J.R. Ehleringer, Responses of boreal conifers to climate fluctuations: indications from tree-ring widths and carbon isotope analyses, Can. J. For. Res. 28 (4) (1998) 524–533.
[63] J. Huang, J.C. Tardif, Y. Bergeron, B. Denneler, F. Berninger, M.P. Girardin, Radial growth response of four dominant boreal tree species to climate along a latitudinal gradient in the eastern canadian boreal forest, Glob. Change Biol. 16 (2) (2010) 711–731.
[64] C. Grossiord, A. Granier, A. Gessler, T. Jucker, D. Bonal, Does drought influence the relationship between biodiversity and ecosystem functioning in boreal forests?, Ecosystems 17 (2014) 394–404.
[65] C. Ammer, Diversity and forest productivity in a changing climate, New Phytol. 221 (1) (2019) 50–66.
[66] J.W. Kantelhardt, E. Koscielny-Bunde, D. Rybski, P. Braun, A. Bunde, S. Havlin, Long-term persistence and multifractality of precipitation and river runoff records, J. Geophys. Res. 111 (D1) (2006).
[67] M. Bogachev, A. Bunde, Universality in the precipitation and river runoff, Europhys. Lett. 97 (4) (2012) 48011.
[68] A. Bunde, M.I. Bogachev, S. Lennartz, Precipitation and river flow: long-term memory and predictability of extreme events, in: Extreme Events and Natural Hazards: The Complexity Perspective, vol. 196, 2012, pp. 139–152.
[69] C.L. Franzke, S. Barbosa, R. Blender, H.-B. Fredriksen, T. Laepple, F. Lambert, T. Nilsen, K. Rypdal, M. Rypdal, M.G. Scotto, et al., The structure of climate variability across scales, Rev. Geophys. 58 (2) (2020) e2019RG000657.
[70] K. Fraedrich, R. Blender, Scaling of atmosphere and ocean temperature correlations in observations and climate models, Phys. Rev. Lett. 90 (10) (2003) 108501.
[71] R. Blender, K. Fraedrich, F. Sienz, Extreme event return times in long-term memory processes near 1/f, Nonlinear Process. Geophys. 15 (4) (2008) 557–565.
[72] M. Bogachev, J. Eichner, A. Bunde, The effects of multifractality on the statistics of return intervals, Eur. Phys. J. Spec. Top. 161 (1) (2008) 181–193.
[73] M.I. Bogachev, J.F. Eichner, A. Bunde, On the occurence of extreme events in long-term correlated and multifractal data sets, Pure Appl. Geophys. 165 (2008) 1195–1207.